
Article:
Lira, C., Scarpa, F., Tai, Y.H. et al. (1 more author) (2011) Transverse shear modulus of SILICOMB cellular structures. Composites Science and Technology, 71 (9). pp. 1236-1241. ISSN 0266-3538

https://doi.org/10.1016/j.compscitech.2011.04.008

Transverse shear modulus of SILICOMB cellular structures

C. Lira, F. Scarpa, Y.H. Tai, J.R. Yates

PII: S0266-3538(11)00141-2
DOI: 10.1016/j.compscitech.2011.04.008
Reference: CSTE 4969

To appear in: *Composites Science and Technology*

Received Date: 27 January 2011
Revised Date: 6 April 2011
Accepted Date: 8 April 2011

Please cite this article as: Lira, C., Scarpa, F., Tai, Y.H., Yates, J.R., Transverse shear modulus of SILICOMB cellular structures, *Composites Science and Technology* (2011), doi: 10.1016/j.compscitech.2011.04.008

Transverse shear modulus of SILICOMB cellular structures

C. Lira, F. Scarpa

Advanced Composites Centre for Innovation and Science, University of Bristol, Bristol BS8 1TR, UK

Y. H. Tai

Department of Mechanical Engineering, University of Sheffield, Sheffield S1 3JD, UK

J. R. Yates

MACE, University of Manchester, Manchester M60 1QD, UK

Abstract

This work describes the transverse shear stiffness properties of a novel honeycomb with zero Poisson's ratio. The cellular configuration is simulated using a series of finite element models representing full-scale and representative unit cells of the honeycomb topology. The models are benchmarked against experimental results from pure shear and 3-point bending ASTM tests. The benchmarked models are used to perform a parametric study of the shear moduli (G_{13} and G_{23}) against the geometry of the unit cell and the gauge thickness of the honeycomb panels. The shear stiffness maps obtained allow comparison of the SILICOMB configuration against classical centresymmetric and rectangular honeycomb topologies.

Keywords: A. sandwich; B mechanical properties; C. sandwich structures; C. elasticity;

1. Introduction

Cellular structures are known for their large variation of Poisson's ratio value, due to the geometry and stiffness distributions of their cell walls [1]. The classical hexagonal regular honeycomb has an in-plane Poisson's ratio of 1, when its unit cell ribs deform under pure bending [1]. Other centresymmetric hexagonal configurations can exhibit either positive or negative (auxetic) Poisson's ratio values [2, 3, 4, 5]. Negative Poisson's ratio (NPR) has been also observed in chiral (non-centresymmetric) configurations [6, 7, 8], although some specific tessellations exhibit the NPR effect only under nonlinear deformations [9]. A particular subset of cellular structures is the one possessing a *zero* Poisson's ratio. Zero ν implies that the material does not deform laterally when subjected to mechanical loading (tensile or compressive). **The so-called**

Email address: f.scarpa@bristol.ac.uk (C. Lira, F. Scarpa)

"ox-core" honeycombs (highly elongated hexagonal cores) have been traditionally used as honeycomb structures with quasi-zero ν properties [10]. Cellular materials with zero Poisson's ratio have also been proposed for one-dimensional spanwise morphing of wings and blades [11, 12], as well as scaffolds for biomedical applications [13]. The zero ν characteristics also offers the possibility to manufacture tubular structures with absence of sinclastic or anticlastic behaviour [14]. The presence of a zero ν has been observed in cork [1], liquid crystalline polymers [15], but also in cellular structures such as the accordion honeycombs [12]. Square honeycombs have an in-plane Poisson's ratio proportional to the product between the relative density and the Poisson's ratio of the core material, leading to a virtually zero ν for small relative densities ($\sim 2 \div 3$ %) [16]. Grima and co-workers have recently proposed cellular configurations based on semi-re-entrant layouts providing alternate conventional - auxetic layers with zero ν effect [14, 17]. Another contribution to the field of zero-ν cellular materials is the SILICOMB configuration considered in this work, which has been developed by some of the Authors [18]. The SILICOMB layout features a topology inspired by the tessellation of β- crystobalite lattice [19, 20], leading to a cellular in-plane orthotropic configuration, with a Poisson's ratio ν_{21} equal to zero, **a behaviour which has been confirmed also by experimental tests** [18].

With the exception of rectangular honeycombs [16, 21], the zero Poisson's ratio cellular layouts have been evaluated only under in-plane mechanical loading, and no data exist about the transverse shear stiffness of zero-ν honeycombs. However, for classical sandwich structures constructions, the transverse shear modulus is a primary factor determining the out-of-plane bending deflection of a plate [22]. In this work, the transverse shear moduli related to various SILICOMB cellular configurations are investigated for the first time using numerical and experimental techniques. Full-scale and Representative Volume Elements (RVE) of SILICOMB topologies are developed using Finite Elements (FE), with boundary conditions representing pure shear and homogenization of periodic microstructures [23]. The FE models are fully parametrised, and allow identifying the dependence of the shear moduli versus the geometric configurations of the honeycomb unit cells. Honeycomb samples have been produced using Rapid Prototyping techniques according to dimensions compatible with cellular panels for transverse shear tests, and as cores for sandwich beams to be tested under 3-point bending loading. The experimental results have been instrumental in benchmarking the FE models developed, which have been then used to perform a parametric analysis of the SILICOMB configurations, and compare them with existing honeycomb topologies.

2. Models and experimental results

2.1. Geometry

Figure 1 shows a representative unit cell of the SILICOMB configuration. The RVE is composed by two walls (l and h) with thickness t, and inclined with two angles (ϕ and θ). An auxetic configuration will be obtained with a negative ϕ (as illustrated in Figure 1), while the accordion layout is obtained from $\phi = 0^o$. The thickness of the honeycomb along the 3-direction (Figure 2) is indicated as b. Consistently with other notations used in the Cellular Materials Theory [1], the

mechanical properties of the honeycomb can be expressed using nondimensional parameters (cell wall aspect ratio $\alpha = h/l$, thickness ratio $\beta = t/l$, gauge thickness ratio $\gamma = b/l$), and the material properties of the cell walls (shear modulus G_c and density ρ_c in our case).

2.2. Finite Element models

All numerical models are developed using the commercial code ANSYS 11.0 [24]. The transverse shear properties have been simulated using a full-scale representation of the honeycomb panels under transverse shear [25, 26] and, **as further benchmark,** RVEs with periodic boundary conditions to be used within a FE homogenisation procedure [23, 25]. **Three sets of full-scale FE models were prepared, each having a different type of element. The plate-like elements used** were SHELL63 and SHELL93 elements (four and eight nodes with 6 DOFs respectively), and SHELL28 panels with shear loading capability [24]. Consistently with the work carried out in [25], the use of three different elements for the full-scale shear simulations has been performed to cross-benchmark the models under different geometry and loading conditions. In particular, a full-scale model made with SHELL28 panel quadrilaterals is able to represent the Voigt (upper bound) of the transverse shear modulus in cellular cores [25]. After a mesh convergence analysis, an average mesh size equal to $l/4$ was adopted for the SHELL63 elements, and $l/2$ for the SHELL93 models. The SHELL28 panel elements lose validity when used in shapes other than rectangular. Due to this constraint, the mesh used in the model is limited to one element only along the whole panel depth. For all the full-scale models the boundary conditions have been applied to the bottom and top surfaces along the through-the-thickness (3) direction. At the top surface, each node was subjected to a constant shearing force (linear elastic analysis) along the directions 1 or 2, depending on the type of shear modulus to simulate (G_{13} and G_{23} respectively). At the bottom, all degrees of freedom were clamped. As a close approximation to the effective boundary conditions existing in the experimental test, the degrees of freedom along the loading direction of the nodes belonging to the surface subjected to the shearing force were coupled to translate together as a rigid body (CP command [24]), while the other two translational DOFs were clamped. All the rotational degrees of freedom belonging to the top and bottom surfaces have been blocked to ensure a local stiffening effect existing in the real samples. The total shear stress has been calculated **from** the surface average of the shear force at the top side of the honeycomb, while the equivalent shear strain has been derived from the relative displacement of the nodes between the top and lower surfaces.

The RVEs shown in Figures 3 (a and b) have been used to calculate the equivalent compliance matrix S_{ij} of the homogenised cellular medium, **and developed with brick elements consistently with homogenisation procedures from open literature** [23, 25]. The meshes have been created using 3D 8-nodes hexahedral SOLID45 elements, with two elements along the wall thickness t, and maintaining a constant square aspect ratio. The values of the transverse shear moduli have been calculated from the inversion of the terms S_{44} and S_{55} of the compliance homogenised S_{ij} matrix, obtained through the imposition of periodic boundary conditions and calculation of the second derivative of the strain energy versus the imposed uniform strains [25].

2.3. Manufacturing and experimental tests

The SILICOMB samples were fabricated using a Rapid Prototyping (RP) Fusion Deposition Molding technique (FDM) from Stratasys (Dimension© Elite). The dimensions of the samples used for the transverse shear test are listed in Table 1. Between the nominal input contained in the CAD file and the manufactured parts using the FDM technique, it was possible to observe discrepancies up to 30 %, especially for components below 0.7 mm thickness. The unit cells of the samples had all cell walls with $l = 12$ mm, and average thickness $t = 0.684$ mm. The overall dimensions (L_1 and L_2, along the 1 and 2 directions respectively) have been imposed to satisfy the ASTM C273-07a standard [27].

The SILICOMB samples for the three-point bending test [28] had dimensions 180 mm X 72 mm X 30 mm (Figure 4(a)). The face skins were made using 4 layers of unidirectional prepreg IM7/8552 (Hexcel Corporation), for a total thickness of 0.6 mm. The skins were applied to the FDM cellular cores using a REDUX 810 epoxy adhesive (Hexcel Corporation) and cold-cured for 72 hours.

The material properties of the core (ABS plastic) were determined from dog-bone specimens manufactured with the RP equipment according to the standard test method for tensile properties of plastics (ASTM D638-08). In a previous work the Authors have noticed the significant mechanical anisotropy shown by FDM-made samples, due to the different orientations of the layers arising from the manufacturing process [26]. The Poisson's ratio coefficient has been measured using the strain data recorded along the load direction, and transverse directions using a video extensometer (Messphysik GmbH) with an edge detection system. Consistent with [26], the ABS plastic showed an **anisotropic mechanical behaviour ($E_x = 2016$ MPa, $\nu_x = 0.43$, $E_y = 1530$ MPa, $\nu_y = 0.41$). The layerwise-deposition along two transverse directions typical of FDM techniques should provide a special orthotropic behaviour ($E_x\nu_y = E_y\nu_x$), although the special orthrotropic relation has not been observed in the specimens tested.** The density ($\rho_c = 1040\, kg\, m^{-3}$) has been assumed from the datasheet of the ABS material.

The shear tests were performed using a two-columns electromechanical Instron/Zwick test machine, with BlueHill control and related measuring software. The load cell range (±50 kN) had a relative uncertainty of ±0.22 %. A head displacement rate of 0.50 mm/min was used during the test. The shear panel failure occurred within the core nearby the surface in contact with the test plates, with no apparent debonding. According to the current and previous standards (ASTM-C393-00), a linear curve fit was imposed on the recorded data (**shear stress - shear strain**) to extract the effective shear modulus of the core [27].

The three-point bending tests were performed using an Instron 8501 with a 50 kN load cell (Figure 4(b)). The head was under displacement-control mode at a speed of 0.1 mm/s, and the data acquired with a sampling of 1 Hz. A guide plate was used to prevent the rotation of the actuator during the test. A 2D digital image data correlation system (Davis 7) was used to measure the displacements of the beam parts, with the main deflections obtained from measuring the displacements of the rollers. The tests were conducted at room temperature and under controlled humidity conditions. **The transverse shear modulus G_{13} was calculated firring the measured displacements Δ at different spans to the classical equation for 3-point simply supported sandwich beams with central loading [29]:**

$$\Delta = \frac{W L_b^3}{48\, D} + \frac{W L_b}{4\, A\, G_{13}} \tag{1}$$

Where W is the central concentrated load, L_b the length of the sandwich beam, D the flexural rigidity of the sandwich, and A the cross-section area of the core in the sandwich beam.

2.4. Comparison between experimental and FE results

Table 2 shows the overall comparison between the experimental and numerical results related to the Samples #1 and #2. **It is worth mentioning that in previous in-plane tests Sample #1 has shown an experimental value of ν_{12} equal to 0.05, while the correspondent Poisson's ratio for Sample #2 was -0.03 [18]**. There is a general good agreement between the FE models and the experimental tests, with a difference of 1 % when considering the pure shear loading, and a higher discrepancy (9.6 %) for the 3-point bending test against the homogenised RVE results. The RVE models based on 3D elements have shown a stiffening effect compared to bending, membrane and shear-type shell models representing honeycomb configurations with auxetic behaviour and multi-re entrant (multi-corner) topology [25]. In that sense, a similar behaviour is also expected for the simulations of the SILICOMB configurations, due to the presence of multiple corners in the unit cell geometry. A discrepancy between the shear modulus identified by the pure shear and 3-point bending tests is also expected, considering the way that the core is deformed under bending in a sandwich beam [28, 29]. Regarding the nondimensional shear moduli $G_{13}/G_c/\beta$, the full scale FE shell models based on membrane-bending formulations (SHELL63 and SHELL93) give only a 3.7 % difference against the experimental findings (Table 3). The solid RVE models tend to approach the shear-based full-scale shell representations of the modulus upper bound (SHELL28), both for G_{13} and G_{23}, although for the latter modulus the agreement with the experimental results improves. The experimental results also show a 20 % average decrease of the shear modulus G_{23} compared to the other transverse value. The combined membrane-bending shell models appear to provide a softer mechanical response (20 % lower than the experimental results), while the pure shear-based approach the experimental findings within 3 % and 8 % for Samples 1 and 2 respectively. The dominant contribution of the transverse shear as the main deformation mechanism in the cell walls when loading along the 2-direction can also be understood looking at the geometry of the unit cell (Figure 1), in particular for the configuration with $\phi = 2^o$ (Sample #1). In that case, the two walls having length $h/2$ will be quasi-aligned with the direction of the shear loading, and therefore undergo a pure shear deformation, similarly to the case of the horizontal cell walls in hexagonal honeycombs [1]. From a global point of view, the shell models with combined membrane-bending capabilities provide a reasonable approximation to the experimental findings, although they tend to be conservative for the G_{23} modulus.

3. Parametric analysis

The full-scale validated shell-based membrane-bending models (SHELL63) have then been used to perform a parametric analysis of the transverse shear

moduli against the geometry characteristics of the unit cell. The shear moduli have been non-dimensionalised using G_c and the relative density β, in accordance with the criteria used in [25]. Within the interval of the parameters considered **($-20^o < \theta < 20^o$, $-20^o < \phi < 20^o$, $\beta = 0.05$),** the nondimensional modulus $G_{13}/G_c/\beta$ has maximum values for $\phi = \pm 20^o$ and $\theta = 0^o$, showing a double symmetric distribution of the shear modulus in the (θ, ϕ) plane (Figure 5a). A similar symmetry (albeit with a negative convexity) is observed for the $G_{23}/G_c/\beta$ modulus (Figure 5b), where in this case the maxima are recorded for $\phi = 0^0$, and $\theta = \pm 20^0$. The anisotropy of the SILICOMB cellular configuration is further highlighted by the 73 % increase of the maximum G_{23} value compared to G_{13} at constant relative density β and same core material. **For the distribution of the Poisson's ratios ν_{12} and ν_{21} simulated with a classical lattice finite element model for a similar set of nodimensional parameters, the Reader can consult Reference [18].**

It is interesting to notice the dependence of the transverse shear moduli versus the gauge thickness ratio γ. In Figures 6a and 6b the transverse moduli are normalised against the upper shear modulus G_U identified at $\gamma = 1$, which provides a good approximation with the Voigt upper bound in hexagonal centresymmetric cellular structures [2]. In hexagonal honeycombs, the G_{13} modulus is independent of the gauge thickness. On the other hand, in-plane bending deformation of the cell walls does affect the shear stiffness of the hexagonal honeycomb along the $(2, 3)$ plane, with a linear dependence of the modulus G_{23} versus γ^{-1} between the lower (Reuss) and upper bounds [30, 2]. The SILICOMB configurations show a peculiar behaviour, where a gauge thickness dependence exist for both shear moduli. For the case of G_{13}, one can observe a decrease a 31 % decrease of the normalised modulus from $\gamma = 1.25$ to $\gamma = 11$ (Figure 6a), as the G_{23}/G_U ratio (Figure 6b). It is worth noticing that the behaviour of the nondimensional moduli is not dependent on the geometric configuration of the unit cells. A possible explanation of why the G_{13} modulus is dependent on the gauge thickness can be ascertained by looking at the geometry of the unit cell. In hexagonal honeycombs, the walls perpendicular to the direction 1 in Figure 1 are comprised horizontal plates [1]. The Voigt and Reuss bounds can be calculated imposing shear displacements and shear strain respectively (theorems of minimum potential and minimum complementary energy [1, 25]). When loading along the 1-direction, classical hexagonal honeycombs have their horizontal cells deforming under pure bending, with only the oblique cells providing shear resistance. The shear flow (both in terms of strains and stresses) provides unique linear elastic response of the cellular material, with a single equivalent shear modulus (upper and lower bounds do coincide). With the SILICOMB configuration, the walls transverse to the 1-direction are not horizontal, but included by an angle ϕ. The walls with length $h/2$ (Figure 1) will be therefore subjected to a combination of shear and bending deformations, leading to a non-unique value of shear modulus, and the presence of upper and lower bounds as in the case of hexagonal honeycombs on the $(2, 3)$ plane [1, 30]. Hexagonal centresymmetric honeycombs show approximately the following relation between gauge thickness, and upper and lower (G_L) shear bounds:

$$\frac{G_{23}}{G_U} = \frac{G_L}{G_U} + f(\gamma)\left(1 - \frac{G_L}{G_U}\right) \tag{2}$$

In (2), $f(\gamma) = K/\gamma$, where K varies between 0.787 for positive Poisson's ratio (PPR) configurations, to 1.342 for negative Poisson's ratio (NPR) layouts [2]. Hexagonal centresymmetric honeycombs show a stronger sensitivity to the gauge thickness of the G_{23} shear compared to the SILICOMB layout (Figure 6b), both with configurations with in-plane positive Poisson's ratio (PPR - $\alpha = 2$, $\theta = 20^0$) and negative (NPR - $\alpha = 2$, $\theta = -20^0$) [31, 2]. The SILICOMB configuration appears more sensitive to the thickness along the 3-direction only for $\gamma > 3$, and does not follow the γ^{-1} evolution of Equation (2), but rather the more complex relation:

$$f(\gamma) = a\,\gamma^{-b} + c \tag{3}$$

Where $a = -0.281$, $b = 0.497$ and $c = 1.261$. The coefficients in (3) have been identified using a least square fitting with a $R^2 = 0.99$ and 95 % confidence level. The lower bound G_U has been approximated from the transverse shear simulations for $\gamma > 20$ [8].

A performance map of the SILICOMB configurations for $\gamma = 4$ against general hexagonal centresymmetric and rectangular honeycombs is shown in Figure 7. For rectangular honeycombs, the transverse shear modulus G_T is equal to [21]:

$$\frac{G_T}{G_c} = \frac{1}{2}\frac{\rho}{\rho_c} \tag{4}$$

The centresymmetric hexagonal configurations have been represented using the transverse shear formulas in [1, 2], for internal cell angles between $-30^o \div 50^o$, and cell wall aspect ratios $0.5 \div 2$. The specific shear moduli $G_{i3}/G_c/\beta/(\rho/\rho_c)$ for the centresymmetric configurations vary between 0.34 to 0.68 for a large range of relative densities $\rho/\beta/\rho_c$ ($0.84 \div 2.4$). The SILICOMB layouts tend to cluster in a much smaller interval ($1.42 \div 1.6$), having however G_{13} specific moduli lower than the hexagonal configurations. The rectangular honeycomb tends to have an higher specific shear stiffness than the SILICOMB when compared against the G_{13} modulus, but on average shows a lower G_{23} than the silica honeycomb of this work. It is also worth noticing the higher value of relative density (2) for the rectangular honeycomb when considered against the SILICOMB geometry.

Conclusions

The zero-ν SILICOMB cellular configuration features special orthotropic mechanical properties, and two transverse shear moduli with unusual characteristics compared to classical centresymmetric hexagonal honeycomb topologies, such as the gauge thickness dependence of G_{13} and G_{23}. Compared to other zero-ν honeycombs like the rectangular one, the SILICOMB offers similar transverse specific shear characteristics (at least for the G_{23} modulus), at 20 % lower density. Moreover, the anisotropy and possible auxetic configuration induced by the combination of the internal cell angles give the SILICOMB cellular platform an higher flexibility in terms of implementation in sandwich structures with complex geometries.

Acknowledgments

This work has been funded through the UK Technology Strategy Board project 16293 REACTICS. The Technology Strategy Board is a business-led executive non-departmental public body, established by the government. Its mission is to promote and support research into, and development and exploitation of, technology and innovation for the benefit of UK business, in order to increase economic growth and improve the quality of life. Please visit www.innovateuk.org for further information. The Authors would like also to thank Miss Emilie Sellez for her help performing the shear experiments. Special thanks go also to the Referees for their useful suggestions.

Reference

[1] L. J. Gibson, M. F. Ashby, Cellular Solids - Structure and properties, Cambridge Solid State Science, Cambridge University Press, 1997.

[2] F. Scarpa, P. J. Tomlin, On the transverse shear modulus of negative Poisson's ratio honeycomb structures, Fatigue & Fracture of Engineering Materials & Structures 23 (2000) 717–720.

[3] T. C. Lim, Functionally graded beam for attaining poisson-curving, Journal of Materials Science Letters 21 (2002) 1899–1901, 10.1023/A:1021688009461.

[4] A. Bezazi, F. Scarpa, C. Remillat, A novel centresymmetric honeycomb composite structure, Composite Structures 71 (3-4) (2005) 356 – 364, fifth International Conference on Composite Science and Technology - ICCST/5.

[5] J. N. Grima, R. Gatt, A. Alderson, K. E. Evans, On the potential of connected stars as auxetic systems, Molecular Simulation 31 (Number 13/November 2005) 925–935(11).

[6] Prall D, Lakes R S, Properties of a chiral honeycomb with a Poisson's ratio -1, International Journal of Mechanical Sciences 39 (1996) 305 – 314.

[7] W. Miller, C. Smith, F. Scarpa, K. Evans, Flatwise buckling optimization of hexachiral and tetrachiral honeycombs, Composites Science and Technology 70 (7) (2010) 1049 – 1056, special issue on Chiral Smart Honeycombs.

[8] A. Lorato, P. Innocenti, F. Scarpa, A. Alderson, K. Alderson, K. Zied, N. Ravirala, W. Miller, C. Smith, K. Evans, The transverse elastic properties of chiral honeycombs, Composites Science and Technology 70 (7) (2010) 1057 – 1063, special issue on Chiral Smart Honeycombs.

[9] A. Alderson, K. Alderson, D. Attard, K. Evans, R. Gatt, J. Grima, W. Miller, N. Ravirala, C. Smith, K. Zied, Elastic constants of 3-, 4- and 6-connected chiral and anti-chiral honeycombs subject to uniaxial in-plane loading, Composites Science and Technology 70 (7) (2010) 1042 – 1048, special issue on Chiral Smart Honeycombs.

[10] Bitzer T, Honeycomb Technology - Materials, Design, Manufacturing, Applications and Testing, Chapman & Hall, London, 1997.

[11] R. Olympio, F. Gandhi, Zero-v Cellular Honeycomb Flexible Skins for One-Dimensional Wing Morphing, in: 48th AIAA/ASME/ASCE/AHS/ASC Structures, Structural Dynamics, and Materials Conference, Honolulu, 2007.

[12] K. R. Olympio, F. Gandhi, Zero Poisson's Ratio Cellular Honeycombs for Flex Skins Undergoing One-Dimensional Morphing, Journal of Intelligent Material Systems and Structuresdoi:10.1177/1045389X09355664.

[13] G. C. Engelmayr, M. Cheng, C. J. Bettinger, J. T. Borenstein, R. Langer, L. E. Freed, Accordion-like honeycombs for tissue engineering of cardiac anisotropy, Nature Materials 7 (2008) 1003–1010.

[14] J.N. Grima, L. Oliveri, D. Attard, B. Ellul, R. Gatt, G. Cicala, G. Recca, Hexagonal Honeycombs with Zero Poisson's Ratios and Enhanced Stiffness, Advanced Engineering Materialsdoi:10.1002/adem.201000140.

[15] Ren, W., McMullan, P. J., Griffin, A. C., Stress strain behavior in main chain liquid crystalline elastomers: effect of crosslinking density and transverse rod incorporation on Poisson's ratio, Physica Status Solidi B 246 (2009) 2124 – 2130.

[16] A. M. Hayes, A. Wang, B. M. Dempsey, D. L. McDowell, Mechanics of linear cellular alloys, Mechanics of Materials 36 (8) (2004) 691 – 713, mechanics of Cellular and Porous Materials.

[17] J.N. Grima, D. Attard, Molecular networks with zero Poisson's Ratio, Physica Status Solidi B 248 (1) (2011) 52–59. doi:10.1002/pssb.201083979.

[18] C. Lira, F. Scarpa, M. Olszewska, M. Celuch, The SILICOMB cellular structure: Mechanical and dielectric properties, Physica Status Solidi B 246 (2009) 2055–2062.

[19] H. Kimizuka, H. Kaburaki, Y. Kogure, Mechanism for Negative Poisson Ratios over the α- β Transition of Cristobalite, SiO_2: A Molecular-Dynamics Study, Phys. Rev. Lett. 84 (24) (2000) 5548–5551.

[20] J. N. Grima, E. Manicaro, D. Attard, Auxetic behaviour from connected different-sized squares and rectangles, Proceedings of the Royal Society A: Mathematical, Physical and Engineering Sciencedoi:10.1098/rspa.2010.0171.

[21] F. Cote, V. S. Deshpande, N. A. Fleck, The shear response of metallic square honeycombs, Journal of Mechanics of Materials and Structures 1 (7) (2006) 1281–1299.

[22] D. Zenkert, The handbook of sandwich constructions, Emas Publishing, 1997.

[23] M. Bornert, T. Bretheau, P. Gilormini, Homogénéisation en mécanique des matériaux 1, HERMES Science Europe Ltd, 2001.

[24] ANSYS Release 11.0 Users Manual, Swanson Inc. Canongsburg, PA (2008).

[25] C. Lira, P. Innocenti, F. Scarpa, Transverse elastic shear of auxetic multi re-entrant honeycombs, Composite Structures 90 (3) (2009) 314 – 322.

[26] C. Lira, F. Scarpa, Transverse shear stiffness of thickness gradient honeycombs, Composites Science and Technology 70 (6) (2010) 930 – 936.

[27] ASTM C273 / C273M - 07a Standard Test Method for Shear Properties of Sandwich Core Materials.

[28] ASTM D7250 / D7250M - 06 Standard Practice for Determining Sandwich Beam Flexural and Shear Stiffness.

[29] Allen H G, Analysis and design of structural sandwich panels, Pergamon Press (Oxford and New York), 1969.

[30] M. Grediac, A finite element study of the transverse shear in honeycomb cores, International Journal of Solids and Structures 30 (13) (1993) 1777 – 1788.

[31] F. Scarpa, P. Panayiotou, G. Tomlinson, Numerical and experimental uniaxial loading on in-plane auxetic honeycombs, The Journal of Strain Analysis for Engineering Design 35 (5) (2000) 383–388. doi:10.1243/0309324001514152.

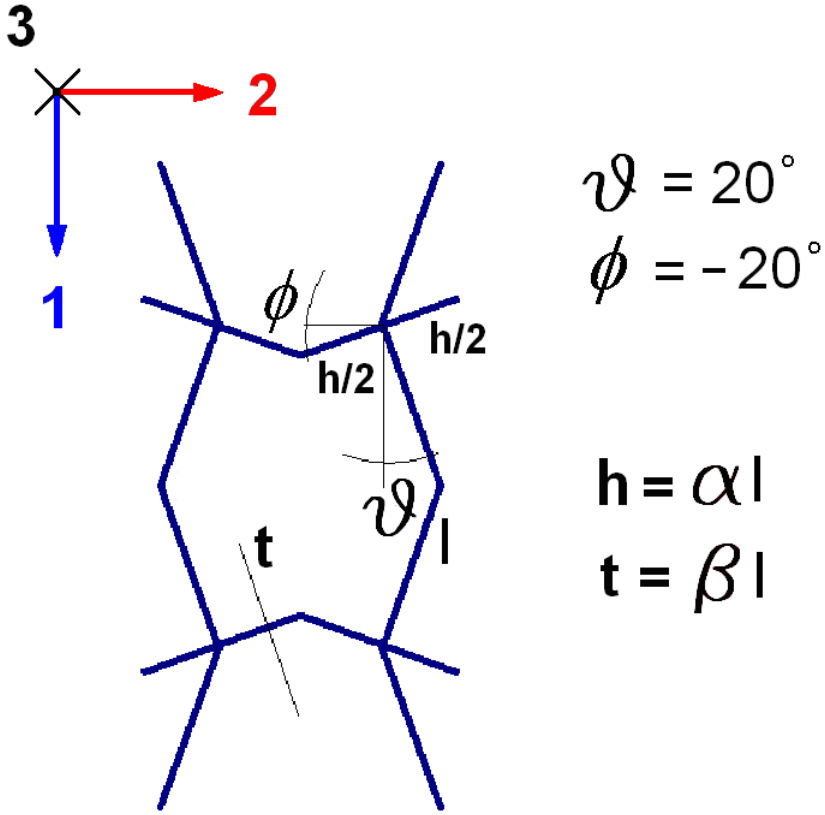

Figure 1: Geometry of the SILICOMB unit cell

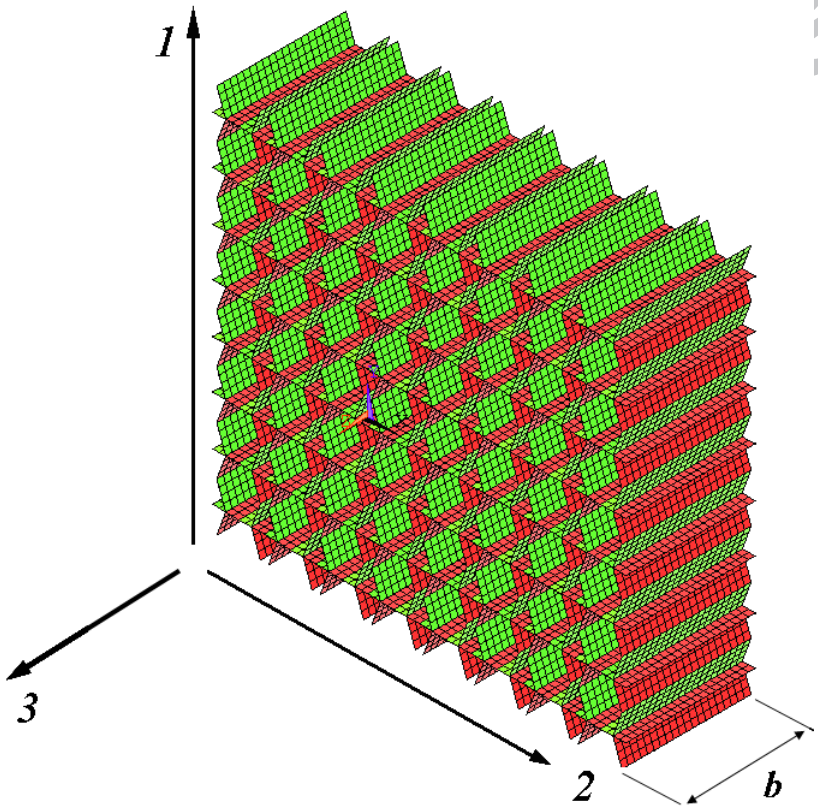

Figure 2: Full scale Finite Element Shell63 model for Sample #1

Sample	#1: $\alpha = 1$, $\beta = 0.057$, $\theta = 20^o$, $\phi = 2^o$, $\gamma = 5$	#2: $\alpha = 1$, $\beta = 0.058$, $\theta = 20^o$, $\phi = -20^o$, $\gamma = 5$
L_1 [mm]	180.5	180.5
L_2 [mm]	192.1	203.3
b [mm]	60.1	60.2
ρ/ρ_c	0.083	0.087

Table 1: Geometry characteristics of the samples for the transverse shear test

Exp. 3-point bending [MPa]	Exp. transverse shear [MPa]	FE Shell63 [MPa]	RVE FE Solid45 [MPa]
31.1	26.8	27.1	34.1

Table 2: Comparison of the shear modulus G_{13} for Sample #1 against the experimental results and numerical models.

	Sample #1		Sample #2	
	$G_{13}/G_c/\beta$	$G_{23}/G_c/\beta$	$G_{13}/G_c/\beta$	$G_{23}/G_c/\beta$
Experimental	0.84	0.68	0.88	0.69
Shell63	0.85	0.54	0.91	0.51
Shell93	0.85	0.54	0.91	0.51
Shell28	0.94	0.66	1.07	0.63
RVE Solid45	0.95	0.61	1.12	0.59

Table 3: Comparison between transverse shear tests and Finite Element models for the two sample. The core material properties are assumed as equal to the geometric mean ($E_c = 1.9$ GPa and $\nu_c = 0.42$).

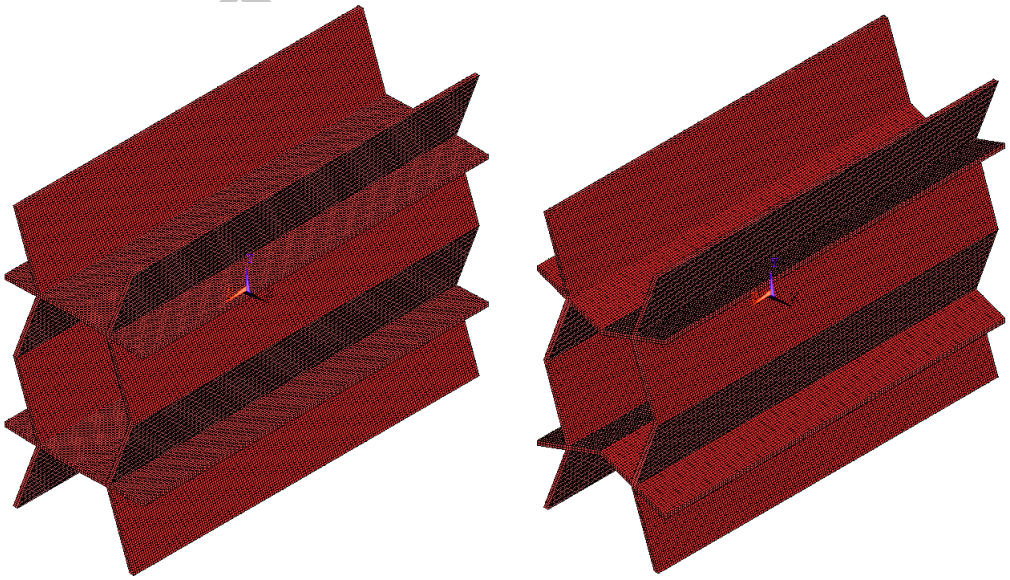

(a) $\alpha = 1$, $\theta = 20^o$, $\phi = 0^o$ (b) $\alpha = 1$, $\theta = 20^o$, $\phi = -20^o$

Figure 3: Representative Unit Volumes (RVEs) for FE homogenisation.

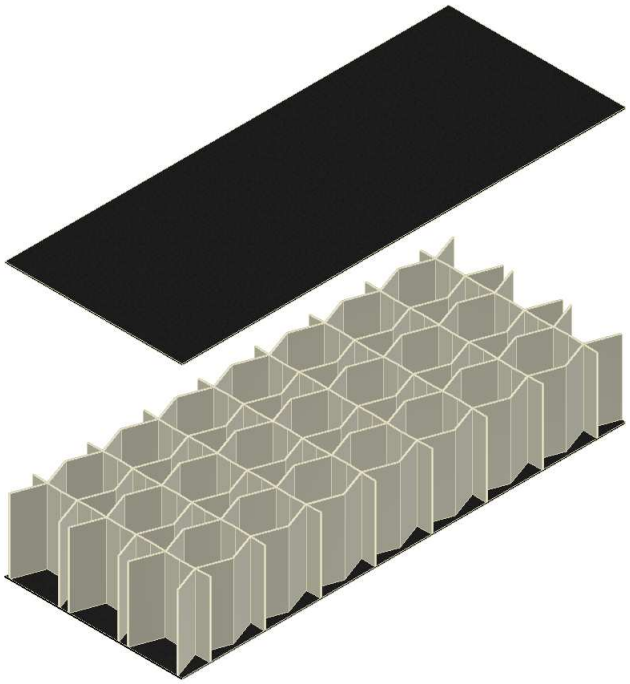

(a)

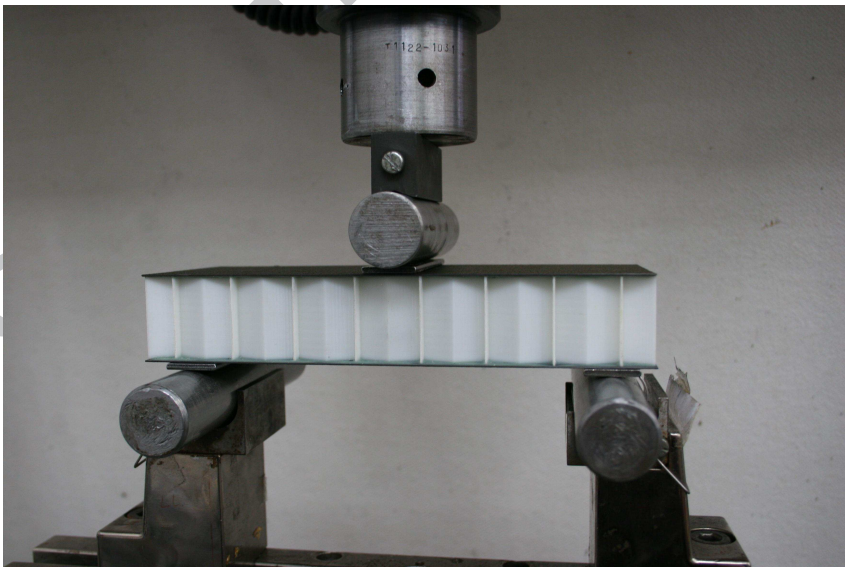

(b)

Figure 4: (a) sandwich beam for three-point-bending and (b) test setup.

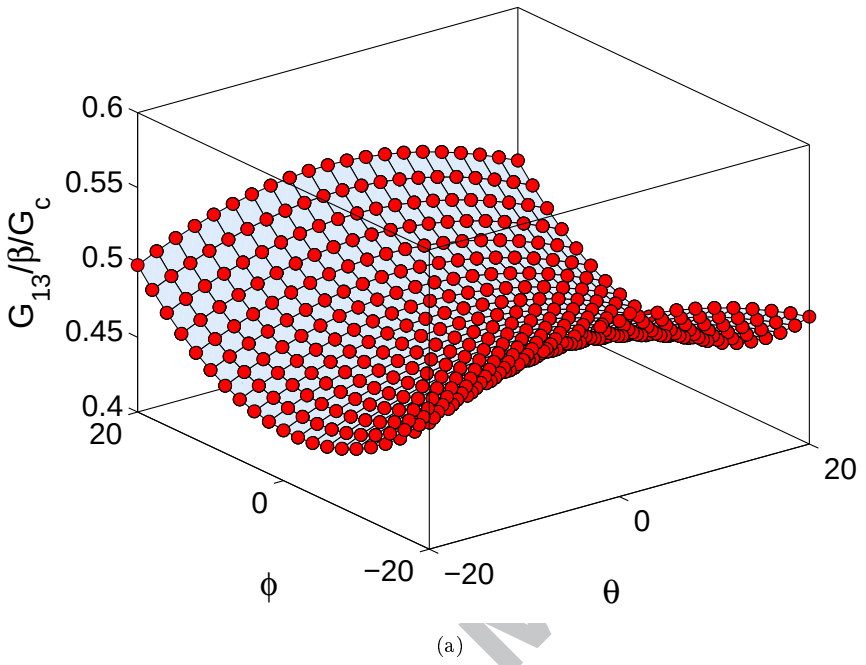

(a)

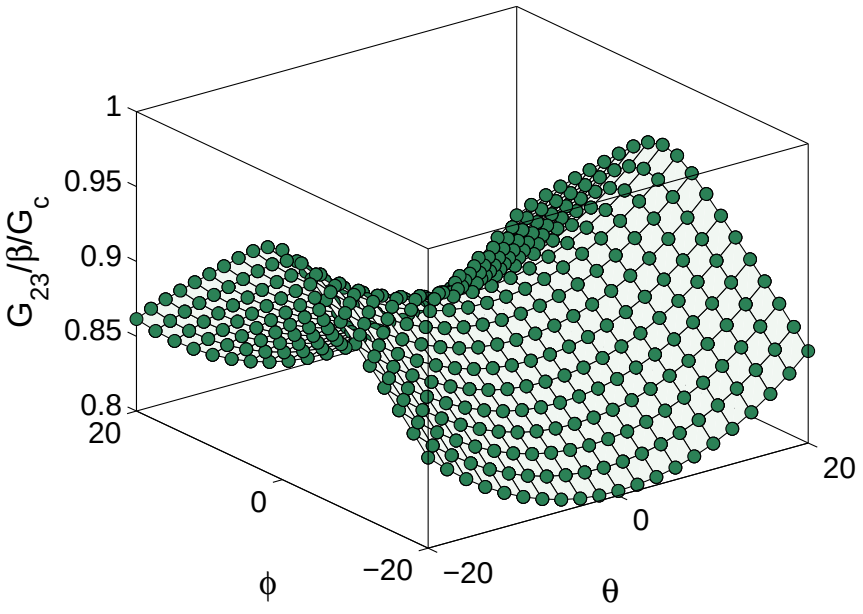

(b)

Figure 5: Nondimensional transverse shear moduli versus the unit cell geometry parameters in the (a) 13 and (b) 23 planes. The results have been simulated with $\gamma = 5$, $\beta = 0.057$.

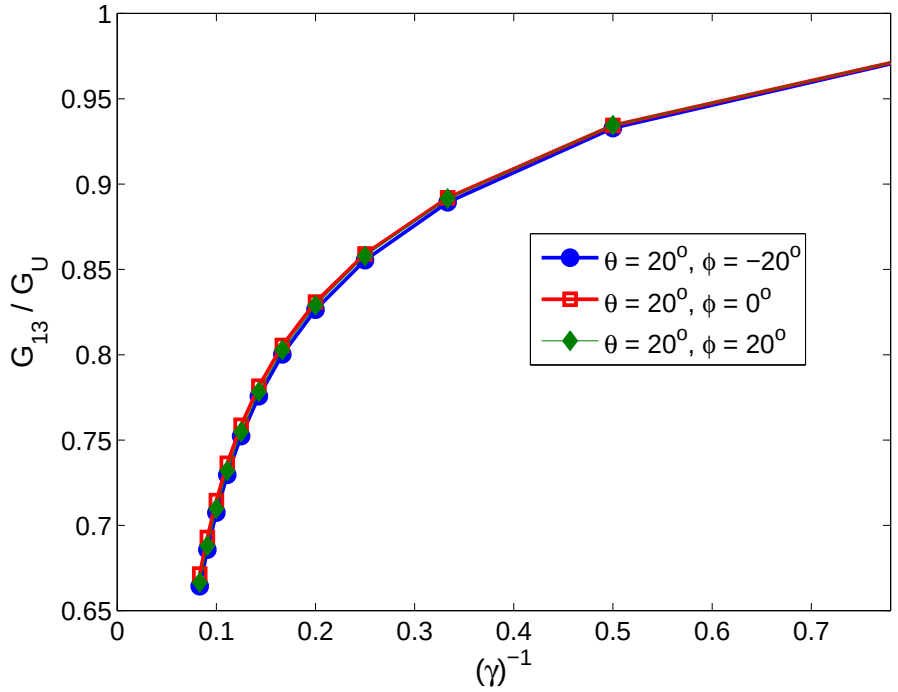

(a)

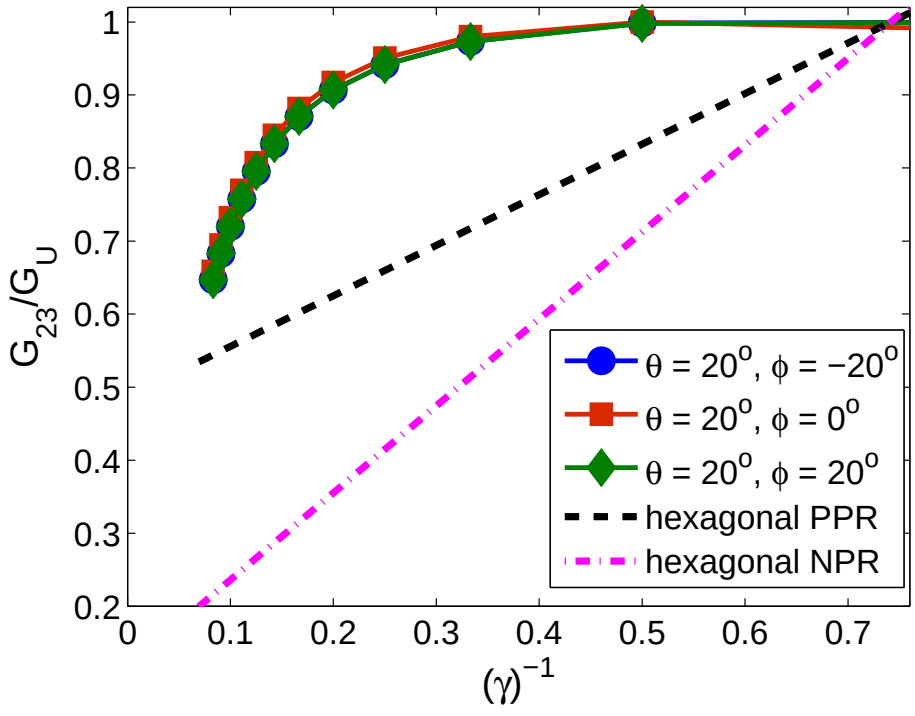

(b)

Figure 6: Normalised transverse shear moduli G_{i3}/G_U $(i = 1, 2)$ versus the gauge ratio γ.

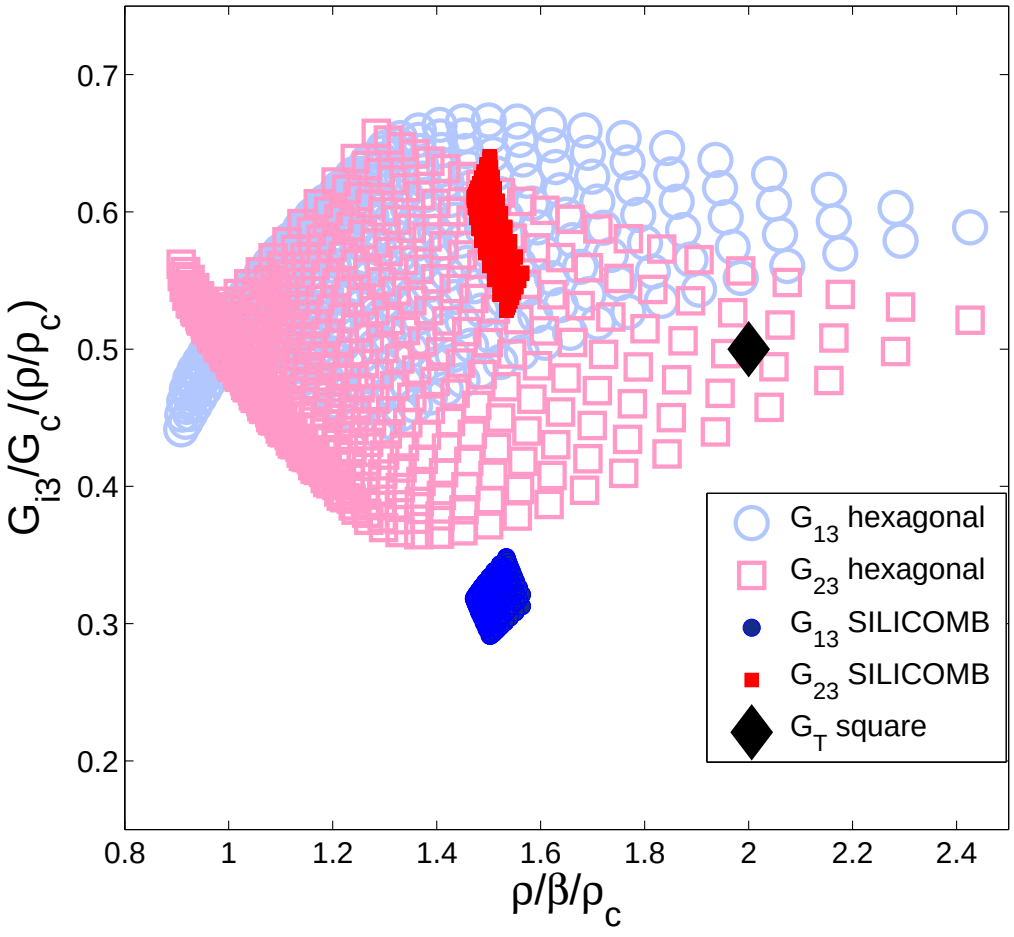

Figure 7: Map of shear moduli normalised against the relative density for hexagonal, SILICOMB and square cell honeycomb configurations. The gauge ratio is constant for all cases ($\gamma = 4$).